InGaAs based heterojunction phototransistors: Viable solution for high-speed and low-noise short wave infrared imaging F

Mohsen Rezaei, Min-Su Park, Cobi Rabinowitz, Chee Leong Tan ⬦, Skylar Wheaton, Melville Ulmer, and Hooman Mohseni

COLLECTIONS

F   This paper was selected as Featured

View Online   Export Citation   CrossMark

InGaAs based heterojunction phototransistors: Viable solution for high-speed and low-noise short wave infrared imaging Ⓕ

Mohsen Rezaei,[1,a)] Min-Su Park,[1,2,a)] Cobi Rabinowitz,[1,3] Chee Leong Tan,[1,4] (iD) Skylar Wheaton,[1] Melville Ulmer,[3] and Hooman Mohseni[1,b)]

AFFILIATIONS

[1]Bio-Inspired Sensors and Optoelectronics Laboratory, Northwestern University, 2145 Sheridan Rd, Evanston, Illinois 60208, USA
[2]Nano Convergence Research Center, Korea Electronics Technology Institute (KETI), 111, Ballyong-ro, Deokjin-gu, Jeonju-si, Jeollabuk-do 54853, South Korea
[3]Department of Physics and Astronomy and CIERA, Northwestern University, 2131 Tech Drive, Evanston, Illinois 60208-2900, USA
[4]Photonics Research Center, University of Malaya, 50603 Kuala Lumpur, Malaysia

[a)]Contributions: M. Rezaei and M.-S. Park contributed equally to this work.
[b)]Author to whom correspondence should be addressed: hmohseni@northwestern.edu.

ABSTRACT

Highly sensitive and fast imaging at short-wavelength infrared (SWIR) is one of the key enabling technologies for the direct-imaging of habitable exoplanets. SWIR imaging systems currently available in the market are dominated by imagers based on InGaAs PIN photodiodes. The sensitivity of these cameras is limited by their read-out noise (RON) level. Sensors with internal gain can suppress the RON and achieve lower noise imaging. In this paper, we demonstrate a SWIR camera based on 3D-engineered InP/InGaAs heterojunction phototransistors with responsivities around 2000 A/W which provides a shot-noise limited imaging sensitivity at a very low light level. We present the details of the semiconductor structure, the microfabrication, and the heterogeneous integration of this camera. The low capacitance pixels of the imager achieve 36 electron effective RON at frame rates around 5 kilo-frames per second at an operating temperature of 220 K and a bias voltage of 1.1 V. This is a significant step toward achieving highly sensitive imaging at SWIR at high frame rates and noncryogenic operating temperatures. Based on the proposed modeling and experimental results, a clear path to reach the RON less than 10 electrons is presented.

Published under license by AIP Publishing. https://doi.org/10.1063/1.5091052

Information carried by photons is the most prominent way to understand the Universe. The invention of cameras revolutionized our way of life by recording this vast amount of information in a highly parallel fashion. Visible wavelength imagers, which use silicon technology, have recently achieved the ultimate sensitivity of single-photon detection.[1] The immediate wavelength range above the visible is called short-wavelength infrared (SWIR) and is of great interest to astronomy[2] and many other fields such as medical imaging,[3] light detection and ranging (LiDAR), and quantum computing.[4,5] Although the noise performance of SWIR imagers has dramatically improved in the last few decades, they are still not as sensitive as visible imagers.

Commercial SWIR imaging sensors are dominated by InGaAs PIN photodetectors. The sensitivity of these cameras is limited to their read-out noise (RON) which is noise generated by the electronic circuits reading photo-induced charges produced by the detectors. The RON increases with the frame rate and hence the sensitivity of imagers deteriorates at higher frame rates. For detectors without an internal gain such as PIN photodetectors, lowering the operating temperature beyond a certain point no longer reduces their noise levels because the RON starts to become dominant. We can adapt photodetectors with internal gain to make detection systems that their sensitivities are not limited by read noise. Phototransistors are one of the prominent options that use transistor action as their internal gain mechanism. Researchers have made a tremendous effort in the realization of different types of phototransistors. These devices cover detection wavelengths ranging from the infrared to ultraviolet region of the electromagnetic spectrum.[6–9]

This article presents a demonstration of a SWIR camera based on InP/InGaAs heterojunction phototransistors (HPTs). We developed a 3D-engineered InP/InGaAs HPT with a responsivity gain of ∼2000 electrons per photon and a noise equivalent photon (NEPh) of ∼36 at

~5000 frames per second. We present evidence that shows that the special geometry of our 3D-engineered HPT enables such a high sensitivity. Previously, we showed that the sensitivity of HPTs is mainly determined by their effective capacitance at the base layer.[10,11] Based on this insight, an optimal structure for a HPT with high sensitivity is demonstrated for an imager with a 320×256 focal plane array (FPA) with a $30\,\mu$m pixel pitch. The fabricated detector array is integrated with an off-the-shelf CMOS read-out integrated circuit (ROIC) (ISC9705, FLIR) with 575–870 e-rms noise in different settings. Measurement results show that 3D-engineered detectors eliminate the noise generated by the ROIC so that the demonstrated SWIR imager reaches a shot noise limited performance at ultralow power.

Figure 1 shows the schematic diagram of a pixel with a 3D-engineered HPT. The emitter, base, and collector layer of the pixel are shown with different colors in the figure. In the proposed HPT structure, the base and emitter areas are much smaller than the collector area. The goal is to reduce the overall junction capacitance at the base layer while having the large enough collector area to allow better light coupling to reduce the required numerical aperture for the microlens array. Based on our previous work,[10] the total capacitance at the base junctions is the main factor that determines the sensitivity of the HPT.

For imaging applications, we can use the noise equivalent photon (NEPh), defined as the minimum number of photons per frame at a given frame rate that can generate a signal with SNR = 1, as the measure of detector sensitivity.[12] For higher speed applications such as optical communications, other performance measures such as SNR are also used.[13] The NEPh of a typical phototransistor in low-light conditions is given by[10]

$$NEPh = \frac{1}{\eta} \cdot \frac{\gamma F}{2} \cdot \left(1 + \sqrt{1 + \frac{8}{\gamma F}\frac{C_T}{C_0}}\right), \qquad (1)$$

where C_T is the total capacitance at the base and C_0 is the thermal capacitance expressed by

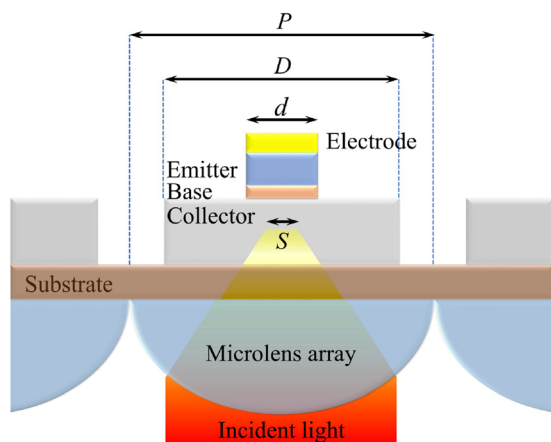$$C_0 = \frac{q}{V_t} = \frac{q^2}{kT}. \qquad (2)$$

FIG. 1. Schematic diagram of a single pixel consisting of the 3D engineered-HPT sensor and a microlens array.

In this equation, q is the charge quanta and V_t is the thermal voltage given by $V_t = kT/q$, where T is the temperature and k is the Boltzmann constant. F, γ, and η are the excess noise factor, Fano factor,[14–16] and quantum efficiency, respectively. Due to the charge number fluctuation at the base, F is predicted to be equal to two for phototransistors.[17] The nature of the excess noise in phototransistors is different from that in avalanche photodiodes (APDs). APD's excess noise is due to the stochastic nature of the impact ionization which is temperature dependent,[18] while the excess noise in phototransistors is due to adding two independent shot noise currents and has no dependence on temperature.[17] The Fano factor is a convenient way of evaluating a non-Poissonian shot noise. A recently studied EI detector—HPT with type-II band alignment—exhibited a Fano factor of 0.5 at a 1 V bias voltage.[15] Also, in Ref. 16 for an InGaAs pn junction, the Fano factor is measured to be around 0.3. These measured low values of the Fano factor could be due to the negative feedback within the devices which favors antibunching of the majority carriers traveling through the base. Therefore, in this paper, we assume that the Fano factor is equal to 0.5. Deviations from this number scale our results by the appropriate factor.

Equation (2) clearly shows that it is necessary to decrease C_T in order to increase the sensitivity. One of the most straightforward ways of reducing this capacitance is to decrease the area of the base. However, the pixel pitch is determined by the ROIC pixel pitch and cannot be changed. As a result, the absorption area is significantly larger than the base and regions far from the base may have lower sensitivity to light. Microlens arrays can be employed to increase the efficiency of light coupling into the absorption area near the base as shown in Fig. 1. Consequentially, the proposed HPT pixel has different areas of an electrical part (base and emitter) and an optical part (collector) to have both high sensitivity and fill-factor. Figure 2 shows three SEM images of the detector array and a schematic of the sensor bonded to the ROIC. Part (a) of the figure shows the proposed detector with $d = 4\,\mu$m. In this image, undercut between layers happened due to using a wet etchant in the fabrication process. Here, we first describe the material composition and then briefly outline the fabrication process.

We adapted the HPT structure proposed in Ref. 19. The HPT structure was grown by using a low-pressure metalorganic chemical vapor deposition (LP-MOCVD) system on a 3-in. (001) oriented sulfur-doped InP substrate. Each pixel, from the bottom to the top, consists of a 500-nm-thick n^+-doped ($1 \times 10^{19}\,cm^{-3}$) InP buffer layer, a 25-nm-thick n^--doped ($5 \times 10^{15}\,cm^{-3}$) InGaAsP compositional graded layer, a 1.5–μm-thick n^--doped ($1 \times 10^{17}\,cm^{-3}$) InGaAs collector layer, a 100-nm-thick p^--doped ($2 \times 10^{17}\,cm^{-3}$) InGaAs base layer, a 25-nm-thick undoped InGaAsP spacer layer, a 200-nm-thick n^-–doped ($1 \times 10^{16}\,cm^{-3}$) InP emitter layer, a 50-nm-thick n^--doped ($1 \times 10^{16}\,cm^{-3}$) InGaAsP step graded layer, and a 300-nm-thick n^+–doped ($1 \times 10^{19}\,cm^{-3}$) InGaAs cap layer. Zinc and silicon are used as the p-type and n-type dopants, respectively. The described structure can be further optimized for a smaller overall capacitance at the base layer. For example, decreasing the doping level of the emitter layer and increasing its thickness can help to decrease the emitter-base junction depletion capacitance.

For the fabrication of the sensor array, the emitter and base layers were selectively removed by chemical wet etchants with the metal mask so that pillar structures were built up. Each pixel with an area of
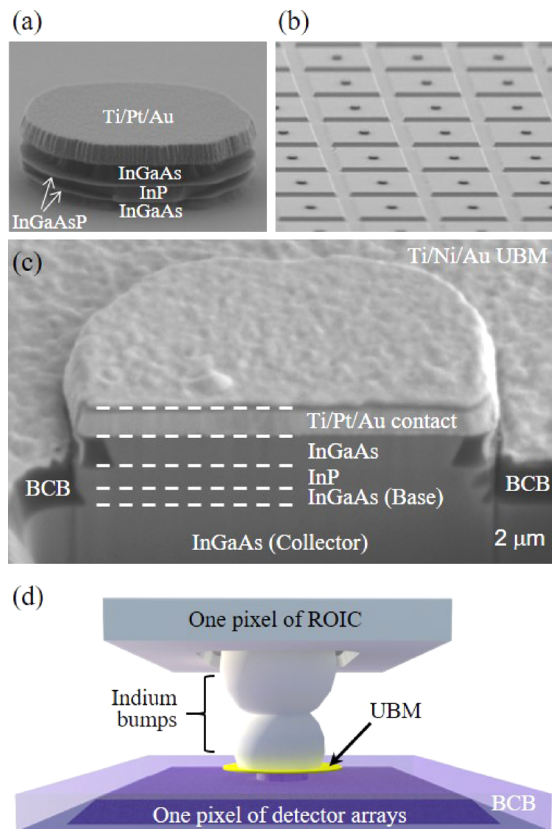
FIG. 2. (a) SEM image of the pillar structure consists of a Ti/Pt/Au contact layer followed by the emitter, base, and collector layers fabricated by a wet etching process. (b) Log magnification image of the array of sensors before planarization. (c) Cross-sectional image of the pixel after planarization with the BCB polymer. (d) Schematic image of the sensor bonded to the ROIC with indium bumps.

$26 \times 26 \ \mu m^2$ and a pitch of $30 \ \mu m$ was defined by photolithography and an isolation etching using a wet etchant. A planarization process is critical for the indium bump bonding since the 3D-engineered HPT does not have a large enough surface to support the indium bumps. The bisbenzocyclobutene (BCB) polymer was spin-coated and cured at $250\,°C$ for $2\,h$ for the planarization. A BCB etch-back process was conducted using SF_6/O_2 chemistry etching until the top electrodes are exposed and secured as a location to form indium bumps on them. A Ti/Ni/Au (20/30/100 nm) scheme was utilized for under bump metallization. A thin Au seed layer was sputtered on the whole surface of the sample for indium electroplating. A 10-μm-diameter open patterning using a double coating of a thick photoresist gave rise to around 6-μm-height indium pillars after the electroplating. A reflow process was conducted in a liquid flux at $160\,°C$, resulting in dome-shaped indium bumps on each pixel. The same process for forming one indium bump per pixel was applied to CMOS-based ROIC. Finally, the detector arrays were combined with the ROIC by indium interconnection, implementing the hybrid architecture for the SWIR sensor.

We have made multiple detector arrays with sensors with different dimensions. Here, we report the results for a pixel with $d = 2\ \mu m$ and $D = 26\ \mu m$ (see Fig. 1). To characterize the camera, the important

parameters that need to be extracted are the internal gain of the sensor, quantum efficiency, and NEPh. Quantum efficiency is a measure of the effectiveness of an incident radiant flux at producing a measurable current. There are many ways to measure the quantum efficiency for devices without internal gain. The most straightforward way is to measure the response of the photodetector for a calibrated light source. Extraction of quantum efficiency is challenging for detectors with unknown internal gain. The reason is for a detector with quantum efficiency η and current gain of β upon the absorption of N photons, the output signal is given by

$$S_{out} = \eta\beta N. \tag{3}$$

In the literature, the product $\eta\beta$ is called the external quantum efficiency. With only a photoresponse measurement, it would be impossible to decouple these parameters. The gain information can be extracted from the noise content of the detector. Noise analysis gives an unparalleled view to the inside of the detector. The dark current measured at the terminals of a detector with internal gain is called external dark current I_{d-ext} and is given by $I_{d-ext} = \beta I_d$, where I_d is the internal dark current. The noise characteristics of phototransistors have been well studied by others. The output current noise (i_o) of a phototransistor is given by[17]

$$\overline{i_o^2} = 2qI_d \left[1 + \frac{F\gamma\beta}{1 + \left(\frac{f}{f_0}\right)^2} \right] \Delta f, \tag{4}$$

where f_0 is the cutoff frequency given by

$$f_0 = \frac{1}{2\pi\tau}. \tag{5}$$

The time constant of the HPT, τ, can be measured with a great precision by illuminating the detector with a square pulse of light and measuring the rise and fall time [see Fig. 3(a)]. As an illustration, the noise spectrum of the HPT at 220 K is shown in Fig. 3. As shown in this figure, the spectrum of the noise is very similar to what Eq. (4) predicts. Fitting the formula to this result gives $\beta = 1880$. The measured time constant is used to make a better fit for the noise spectrum. This becomes especially important when other sources of noise like flicker noise are visible in the spectrum. Now that we have found the gain we can extract the pixel's quantum efficiency.

Figure 4 shows the histogram of the signal of the aforementioned pixel for a pulse of light with an effective power of 10.7 fW after taking quantum efficiency into account. Since the time constant of the detector is 2.43 ms, it absorbs a total number of 424 photons in the device rise time interval. Considering the SNR = 11.62, this pixel has NEPh = 36.5. Since the ROIC has more than 600 e-noise, achieving 36.5 NEPh means that we have eliminated the ROIC noise.

Figure 5 shows the effect of temperature on the dark current and the noise spectrum of a typical pixel. Increasing the temperature increases both the dark current and the speed of the detector. The increase in the speed due to the increase in the internal dark current is predicted by our model.[10] The figure also shows that the responsivity decreases at higher temperatures. Responsivity is given by the ratio of the minority carrier lifetime at the base layer to the electron transit time through the base layer. Decreasing temperature increases the carrier lifetime and hence increases the gain of the detector.
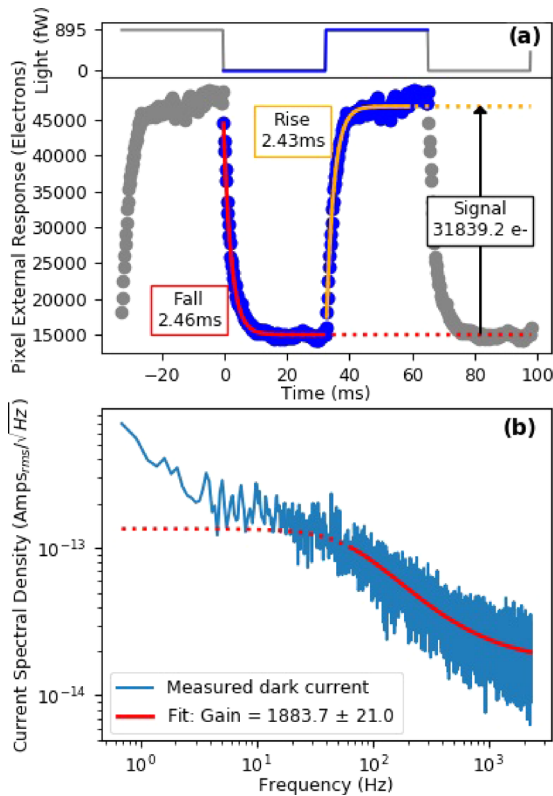
FIG. 3. (a) Response of a pixel to a square-wave light pulse of 895 fW, spread uniformly across the pixel surface with a $26 \times 26~\mu m^2$ area. Frames were taken at 4590 Hz with a 202 μs integration time. The pulse and frame rates were synchronized to allow averaging; shown is 50 averaged responses. Exponentials were fit to the rise and fall to find the pixel's response time. (b) Noise spectrum of the same pixel. Shown is the average of the Fourier analyses of 10 runs of 10 000 consecutive dark frames each, all taken at 4590 Hz with 202 μs integration. Equation (4) with $F\gamma = 1$ was fit to the spectrum, using $f_0 = 65.5$ Hz and dark current $I_{d-ext} = 2.3 \times 10^{-11}$ A. The fit yielded an internal current gain β of 1883 ± 11.1.
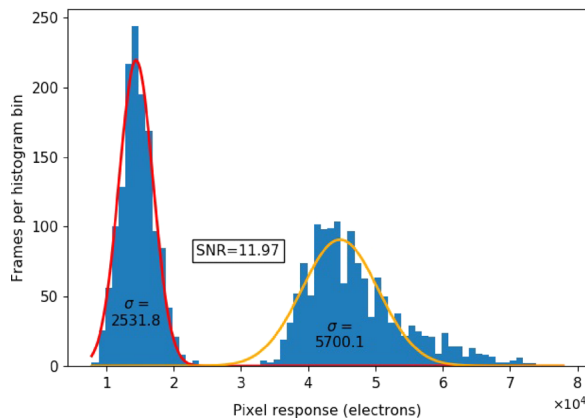

FIG. 4. Histogram of the same pixel as in Fig. 3 for the illumination with a pulse of light with an effective power level of 10.7 fW.
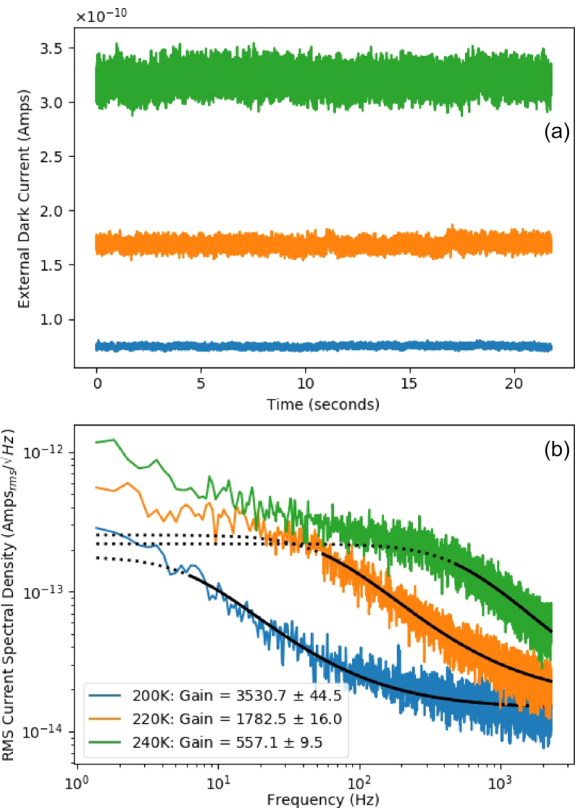

FIG. 5. (a) Dark current at three different temperatures for a typical pixel. (b) Noise spectrum extracted by taking fast Fourier transform of the dark current data shown in part (a).

For the reported camera based on a 3D-engineered HPT array with $d = 2~\mu m$, we did not remove the substrate, and so, we did not add a microlens array. Instead, we have used an optical focusing system to simulate the micro-lens effect. The numerical aperture of the focusing system was 0.2. Using this system, the measured quantum efficiency was above 60%. Without using this optical system, our quantum efficiency is around 1.2%.

Based on our modeling and experimental work, making HPT sensors with a smaller d would be the next step toward achieving imagers with a lower NEPh. There are other parameters that need to be optimized in order to further enhance the performance of the proposed camera system. We only fabricated detectors with $D = 26~\mu m$, while in theory the size can be optimized to increase the quantum efficiency. The surface treatment and passivation techniques can be adapted to further increase the carrier diffusion length.[20] It is also evident that a custom microlens array can increase the fill factor. In order to add a high numerical aperture microlens on the back of the device, we would need to first remove the substrate.

Our experimental results are in great agreement with our previous theoretical modeling.[10] In that work, as we have explained it before, we claimed that the sensitivity of phototransistors is determined by neither their internal gain nor their dark current but by their capacitance.

Space does not permit a full detailed comparison with other SWIR camera designs based on APDs or milli-Kelvin superconductors.

The InGaAs material used here fills a niche of relatively low cost, volume, and power compared to other approaches. APDs based on III–V structures have not been considered good candidates for imaging applications, due to their high excess noise and dark current. Instead, a tremendous amount of effort has been made to make APD based SWIR imagers using II–VI materials (MCT). While the results from MCT imagers are quite impressive, all reported cameras still need to be operated near 70 K. In parallel, tremendous effort has been made on the design of readout circuits with low noise for PIN detector arrays. The best reported camera based on the PIN InGaAs detector has 30 e-rms noise, thanks to its sophisticated ROIC design, but at about 400 frames per second.

Our modeling shows that reducing the overall junction capacitance at the base layer of HPTs is the main way to increase their sensitivity. We have proposed a 3D-engineered InP/InGaAs HPT sensor and demonstrated a SWIR camera built based on that. Pixel-level performance of this camera shows that we achieved 37 e-noise at around 5000 frames per second. The proposed 3D-engineered HPT based SWIR imager can have a sub-10 NEPh level by reducing d from 2 μm to 500 nm. However, first, we need to overcome some technological challenges on the mechanical stability of the detector structure and uniformity of fabrication.

REFERENCES

[1] J. Ma, S. Masoodian, D. A. Starkey, and E. R. Fossum, Optica **4**, 1474 (2017).

[2] N. Jovanovic, F. Martinache, O. Guyon, C. Clergeon, G. Singh, T. Kudo, V. Garrel, K. Newman, D. Doughty, J. Lozi *et al.*, Publ. Astron. Soc. Pac. **127**, 890 (2015).

[3] G. Hong, J. C. Lee, J. T. Robinson, U. Raaz, L. Xie, N. F. Huang, J. P. Cooke, and H. Dai, Nat. Med. **18**, 1841 (2012).

[4] X. Jiang, M. Itzler, K. O'Donnell, M. Entwistle, M. Owens, K. Slomkowski, and S. Rangwala, IEEE J. Sel. Top. Quantum Electron. **21**, 5 (2015).

[5] J. Zhang, M. A. Itzler, H. Zbinden, and J.-W. Pan, Light: Sci. Appl. **4**, e286 (2015).

[6] C. Soci, A. Zhang, B. Xiang, S. A. Dayeh, D. Aplin, J. Park, X. Bao, Y.-H. Lo, and D. Wang, Nano Lett. **7**, 1003 (2007).

[7] S. Sett, A. Ghatak, D. Sharma, G. P. Kumar, and A. K. Raychaudhuri, J. Phys. Chem. C **122**, 8564 (2018).

[8] N. Yavarishad, T. Hosseini, E. Kheirandish, C. P. Weber, and N. Kouklin, Appl. Phys. Express **10**, 052201 (2017).

[9] J. H. Jung, M. J. Yoon, J. W. Lim, Y. H. Lee, K. E. Lee, D. H. Kim, and J. H. Oh, Adv. Funct. Mater. **27**, 1604528 (2017).

[10] M. Rezaei, M. S. Park, C. L. Tan, and H. Mohseni, IEEE Electron Device Lett. **38**, 1051 (2017).

[11] M. Rezaei, M.-S. Park, C. L. Tan, C. Rabinowitz, S. Wheaton, and H. Mohseni, in *Infrared Technology and Applications XLIII* (International Society for Optics and Photonics, 2017), Vol. 10177, p. 101771O.

[12] A. S. Huntington, M. A. Compton, and G. M. Williams, Proc. SPIE **6771**, 67710Q (2007).

[13] H. Kumar and R. Basu, IEEE Sens. J. **18**, 9180 (2018).

[14] Y. M. Blanter and M. Büttiker, Phys. Rep. **336**, 1 (2000).

[15] O. G. Memis, A. Katsnelson, S.-C. Kong, H. Mohseni, M. Yan, S. Zhang, T. Hossain, N. Jin, and I. Adesida, Opt. Express **16**, 12701 (2008).

[16] Ó. García-Pérez, H. Sánchez-Martín, J. Mateos, S. Pérez, A. Westlund, J. Grahn, and T. González, J. Phys.: Conf. Ser. **647**, 012061 (2015).

[17] F. H. De La Moneda, E. R. Chenette, and A. Van Der Ziel, IEEE Trans. Electron Devices **18**, 340 (1971).

[18] P. J. Ker, J. P. David, and C. H. Tan, Opt. Express **20**, 29568 (2012).

[19] S. W. Choi, S. Furue, N. Hayama, K. Nishida, and M. Ogura, IEEE Photonics Technol. Lett. **21**, 1187 (2009).

[20] M.-S. Park, M. Razaei, K. Barnhart, C. L. Tan, and H. Mohseni, J. Appl. Phys. **121**, 233105 (2017).